OXFORD

*Social Cognitive and Affective Neuroscience*, 2025, **20**(1), nsaf021

DOI: https://doi.org/10.1093/scan/nsaf021
Advance Access Publication Date: 15 February 2025
**Original Research – Neuroscience**

# Decoding affect in emotional body language: valence representation in the action observation network

Johannes Keck[1,2,*], Julia Bachmann[1], Adam Zabicki[1], Jörn Munzert[1,2], Britta Krüger[1]

[1]Nemolab, Institute of Sports Science, Justus-Liebig-University Giessen, Giessen 35394, Germany
[2]Center for Mind, Brain and Behavior (CMBB), Philipps University of Marburg and Justus-Liebig-University Giessen, Marburg 35032, Germany
[*]Corresponding author. Institute of Sports Science, Justus-Liebig-University Giessen, M, Kugelberg 62, 35394 Giessen, Germany.
E-mail: Johannes.keck-2@sport.uni-giessen.de

## Abstract

Humans are highly adept at inferring emotional states from body movements in social interactions. Nonetheless, it is under debate how this process is facilitated by neural activations across multiple brain regions. The specific contributions of various brain areas to the perception of valence in biological motion remain poorly understood, particularly those within the action observation network (AON) and those involved in processing emotional valence. This study explores which cortical regions involved in processing emotional body language depicted by kinematic stimuli contain valence information, and whether this is reflected either in the magnitude of activation or in distinct activation patterns. Results showed that neural patterns within the AON, notably the inferior parietal lobule (IPL), exhibit a neural geometry that reflects the valence impressions of the observed stimuli. However, the representational geometry of valence-sensitive areas mirrors these impressions to a lesser degree. Our findings also reveal that the activation magnitude in both AON and valence-sensitive regions does not correlate with the perceived valence of emotional interactions. Results underscore the critical role of the AON, particularly the IPL, in interpreting the valence of emotional interactions, indicating its essential function in the perception of valence, especially when observing biological movements.

**Keywords:** valence; point light displays; action observation network; social interactions; biological motion

## Introduction

Imagine observing two people from a distance. One person is gesticulating violently, while the other shifts their gaze to the ground. Without even discerning their facial expressions, you quickly form the impression that one person appears to be very angry, whereas the other seems concerned. Simultaneously, you get an idea of the positivity or negativity of the observed scene. This example showcases our astonishing ability to swiftly gather rich information from people's movements, enabling us not only to understand their inner states but also to evaluate them subjectively.

Humans can express and recognize emotions through various channels, including voice, face, and body (de Gelder 2006). In recent years, the study of whole-body emotion expressions referred to as "emotional body language" (EBL) has gained significant prominence in the cognitive sciences (de Gelder 2006, Atkinson et al. 2012, de Gelder et al. 2015, Bachmann et al. 2018). EBL describes the expression of emotion by the body using not only coordinated and distinctive movement patterns associated with certain emotions containing different stereotypical body postures and gestures but also interpersonal and interactional cues (Johansson 1973, De Meijer 1989, Wallbott 1998, Pollick et al. 2001, Clarke et al. 2005, Keck et al. 2022, Atkinson and Vuong 2023).

Neurophysiological research has extensively explored the brain regions involved in the perception and recognition of EBL. These studies have demonstrated convincingly that perceiving emotional bodily expressions involves a large neural network. This network is organized around the action observation network (AON) containing the premotor cortex (PMC), the inferior frontal gyrus (IFG), and the inferior parietal lobule (IPL) and superior parietal lobule (SPL) (Grèzes et al. 2007, Pichon et al. 2009, Kret et al. 2011a, 2011b). Further regions belonging to the AON are the dorsomedial prefrontal cortex, the supplementary motor area (SMA), and regions attuned to bodies (e.g. extrastriate body area and fusiform body area) and biological motion [superior temporal sulcus (STS); see Caspers et al. (2010), Downing and Peelen (2011), Grossman and Blake (2001), and Schwarzlose et al. (2005) for meta-analyses]. Structures involved in emotion and valence processing such as the lateral orbitofrontal cortex (OFC) and amygdala are also activated when perceiving EBL, especially

Received: 29 May 2024; Revised: 17 September 2024; Accepted: 13 February 2025

when full light displays are observed (Gallagher and Frith 2003, Saxe 2006, Carrington and Bailey 2009).

How emotional valence is represented in the human brain has been investigated intensively across various stimulus categories [see Lindquist et al. (2016) for a meta-analysis]. Emotional valence refers to the subjective impression of an object, experience, or scene in terms of its pleasantness or unpleasantness, thereby reflecting its subjective value (Frijda 1986, Kuppens et al. 2013). Neurophysiological studies point to a central role of the OFC (Ongür and Price 2000). Both the lateral and medial OFC regions appear to contain affective representations of stimuli from various modalities (Small et al. 2003, Chikazoe et al. 2014, Lindquist et al. 2016). For instance, the medial OFC and the adjacent ventromedial prefrontal cortices have been linked to reward expectancy, outcome values, and the experience of positive valence. Regarding the preference for negative valence, particularly the left amygdala shows consistent increased activation (Lindquist et al. 2016). However, Lindquist et al. (2016) have suggested a lack of truly valence-specific processing pathways. Instead, they claimed that a flexible affective workspace correlates with positive and negative valence across several brain regions. In this context, Chikazoe et al. (2014) found that neural populations in various brain regions, including the OFC, encode both positive and negative affect.

Despite our advanced understanding of how EBL is processed and how we perceive emotional valence from various types of stimuli, the neural underpinnings that enable humans, as observers, to discern the emotional valence depicted through others' kinematics are still not fully understood. In particular, the roles of specific areas within the AON and regions sensitive to emotional valence require further exploration. This study focuses on two primary objectives: first, we seek to identify which AON and valence-sensitive regions convey valence information when processing EBL depicted by kinematic stimuli. Second, we investigate whether the processing manifests through the magnitude of activation or through distinct patterns within the identified regions of interest by using representational similarity analysis (RSA) and multi-voxel pattern analysis (MVPA). Given the need to infer the emotional content of biological movements exclusively from their kinematics, we hypothesize that certain areas within the AON, which are pivotal for intention recognition from kinematics, play a specialized role in interpreting the emotional valence of the observed stimuli.

# Materials and methods

## Participants

Twenty adults (11 females; mean age: 26.8 years; SD = 5.85 years) with normal or corrected-to-normal vision participated in our study. None reported any history of psychiatric, neurological, immunological or physical disorders, or a current use of psychoactive medication. Prior to participation, all participants gave written informed consent in compliance with the Declaration of Helsinki. The procedure was approved by the local ethics committee of the Department of Psychology and Sports Science of Justus-Liebig-University Giessen.

## Stimuli

Emotional interactions were depicted using point-light displays (PLDs), drawn from a motion-capture dataset developed by Lorey et al. [see Lorey et al. (2012) for full details]. The stimulus set employed here includes 20 emotional PLD interactions that differ in terms of their valence and difficulty. PLD interactions are short-video sequences (4 s, third-person view) showing white dots on a black background with each dot representing specific anatomic landmarks of the actors' bodies covering both upper (shoulders, elbow joints, wrists, and forehead) and lower body parts (hips, knee joints, and ankles) and providing only kinematic information. They depict the movements of two actors portraying one of four emotions: anger, sadness, happiness, and affection. Interactions containing anger and sadness were grouped in the category "negative" emotion, and interactions with affection and happiness were pooled in the category "positive" emotion. Easy stimuli were those interactions on which 91%–100% of viewers agreed on the emotion being portrayed. The difficult stimuli were those with a consensus rate of 50%–70% [see Lorey et al. (2012) for further details].

Additionally, for each stimulus, a scrambled version was created to serve as a control by eliminating form and body information while retaining the dynamic aspects of the motion. These scrambled versions were generated using PLAViMoP software (Decatoire et al. 2019). All stimuli did not differ with respect to their kinematics (see Supplementary Fig. S1).

## Design and task

During fMRI scanning, participants performed six runs of 40 trials employed in an event-related paradigm. Each run contained 10 positive trials (5 easy and 5 difficult) and 10 negative trials (5 easy and 5 difficult). We further added a control condition using a scrambled version of each stimulus. This resulted in a total of 240 trials and a 50-min scanner session overall. Stimuli from all conditions were presented in a pseudorandomized order within each run and counterbalanced across participants. Each trial started with a fixation for 1 s followed by a jitter (0%–90% of Repetition Time (TR) in 10% steps, average 1.5 s) (Fig. 1a). Then PLD or scrambled sequences (4 s) were presented. After observing the sequence, participants were asked to rate the perceived emotional valence on an 11-point Likert scale ranging from −5 ("very negative") to +5 ("very positive") (4 s). After each valence rating, a second rating assessed rating confidence from 0% to 100% confidence (4 s). Figure 1a depicts the whole procedure, except for confidence rating since the analysis presented here was centered on valence perception.

## fMRI: image acquisition

fMRI data were collected on a Siemens Prisma 3-T whole-body scanner (Siemens Prisma, Erlangen, Germany) using a 20-channel head coil. A structural image was acquired from each participant consisting of 176 T1-weighted sagittal images (1-mm slice thickness; MPRAGE) and a fieldmap (40 slices; TR = 1000 ms; Echo Time (TE) = 10 ms). For functional imaging, six runs with 265 volumes per run (i.e. a total of 1590 volumes) were registered using a T2*-weighted gradient echo-planar imaging sequence covering the whole brain with 40 slices (slice thickness = 3 mm; 0.75 mm gap; descending interleaved; TR = 2000 ms; TE = 30 ms; flip angle = 75°; field of view = 210 mm × 210 mm, 2 mm in-plane isotropic resolution). The orientation of the axial slices was parallel to the Anterior Commisure - Posteriore Commisure line. Trial onsets were jittered within 0%–90% of the TR Image.

## Data analysis and statistics

### *Univariate analysis*

Image preprocessing was carried out using SPM 12 (Wellcome Department of Imaging Neuroscience, University College London, UK). Origin coordinates were adjusted to the anterior commissure,

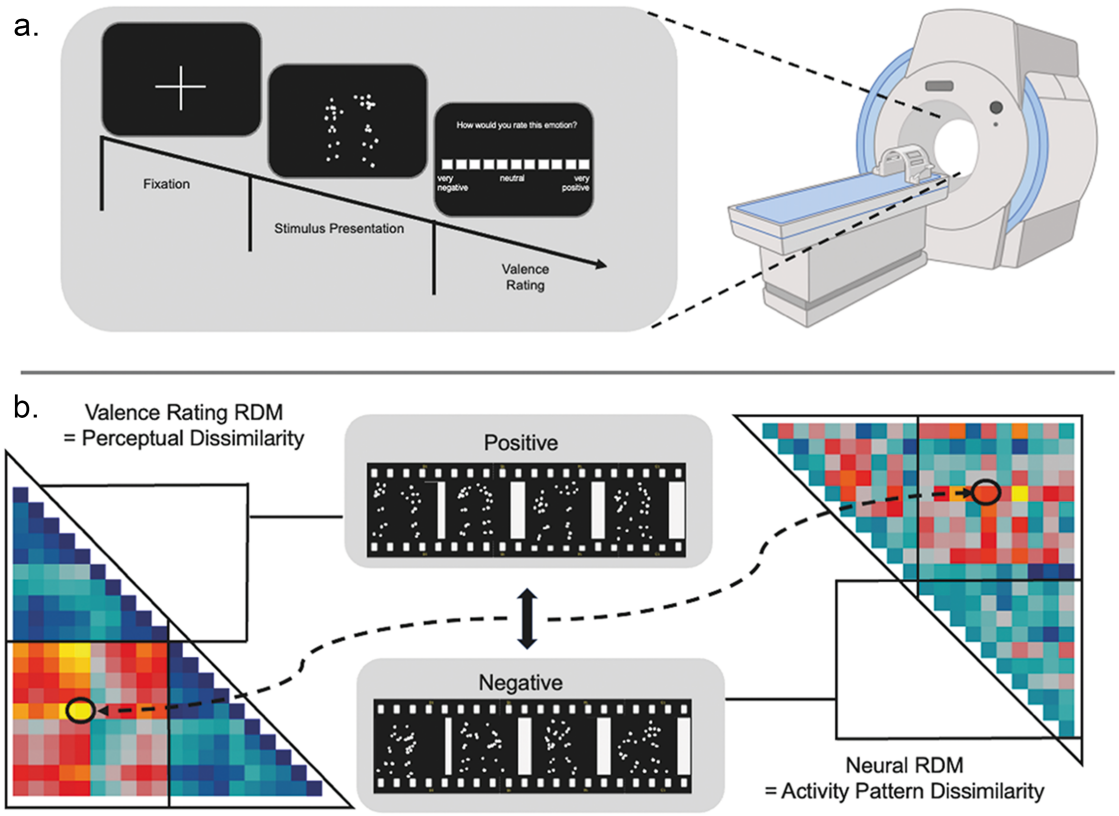


**Figure 1.** Experimental timeline and RDM creation. (a) Temporal structure of one trial. (b) Example interaction of positive and negative scenes (center). In the upper and lower triangle of RDMs, each entry describes the relation between two stimuli. In the main diagonal, the stimuli values are compared with themselves, resulting in a diagonal defined as zeros. In the lower triangle on the left, behavioral RDMs are created by calculating the absolute distance between valence ratings. In the upper triangle on the right neural RDMs are created by calculating the cross-validated Mahlanobis distance between each pair of neural activities. All RDMs are arranged horizontally and vertically in the same order going from positive (10 stimuli) to negative (10 stimuli).

and realignment (2nd Degree B-spline interpolation to the first volume of each functional run) and unwarping were performed using voxel displacement maps generated from the fieldmaps (Hutton et al. 2002). Sinc interpolation was utilized to correct for timing differences in slice acquisition within a single volume. The anatomical data were corrected for B1-field inhomogeneities. Furthermore, the functional images were coregistered with the anatomical scan for each subject. Smoothing was executed with an isotropic three-dimensional Gaussian filter with a full-width-at-half-maximum (FWHM) kernel of 5 mm. Furthermore, normalization to the standard space of the Montreal Neurological Institute brain was performed.

The first-level analysis was computed participant-wise using the general linear model (GLM). A boxcar function was convoluted with the hemodynamic response function. The observation phases for each condition were entered into the model. Boxcar function length covered the respective observation intervals. Moreover, six movement parameters of the rigid-body transformation of the motion-correction procedure were introduced into the GLM as covariates. The voxel-based time series were filtered by a low-pass filter (FWHM = 4 s) and a high-pass filter (time constant = 256 s).

### *Parametric analysis*

Prior to multivariate analysis, we examined brain regions showing increased BOLD signal with increased ratings of emotional valence via a parametric analysis. The parameter values were included as a modulator of the observation regressors representing the main regressor of the GLM. We investigated the hypothesis that valence-sensitive regions would reflect the perceived positivity or negativity of a stimulus. Regarding the modulation of activation magnitude by valence, we tested the positive correlation between the parameter and the brain activation for each participant (the more positive the rated valence, the higher the activation), and vice versa (the more negative the valence rating, the higher the activation). Then, the resulting parameter estimates were entered into a second-level, one-sample *t*-test in which the mean estimate across participants at each voxel was tested against zero (random effects model). The statistical threshold was set at $P = .05$, corrected for multiple comparisons using the family-wise error (FWE) criterion.

### *Multivariate analysis*

#### Regions of interest

The anatomical scan was used to reconstruct the cortical surface of each hemisphere using FreeSurfer (http://surfer.nmr.mgh.harvard.edu). Regions of interest (ROIs) were selected on the basis of previous findings reported in the literature on EBL observation (Caspers et al. 2010, Bachmann et al. 2018) and valence perception (Lindquist et al. 2016). These were defined anatomically on an individual basis using the FreeSurfer parcellation algorithm (Destrieux et al. 2010). We defined 10 ROIs bilateral as follows: "IPL," "SPL," "IFG," "SMAprop," "preSMA," "dorsal PMC (dPMC)," "ventral PMC (vPMC)," and "STS" (AON regions), as well

as "mOFC" and "amygdala" (valence-sensitive regions). Defining ROIs on an individual basis allowed us to work with high anatomic precision and avoided the need for spatial normalization. See Supplementary Table S1 for details on ROI sizes.

### Preprocessing

For the multivariate analyses, we carried out a separate preprocessing. First, realignment and unwarping were performed using voxel displacement maps generated from the fieldmaps (Hutton et al. 2002). The functional images were coregistered with the anatomic scan for the respective subject. Smoothing was executed using an isotropic three-dimensional Gaussian filter with an FWHM kernel of 2 mm.

### General linear models

A first-level analysis was computed with SPM 12 using separate GLMs for each subject and each of the six runs. We created 20 boxcar regressors corresponding to the 10 positive (5 easy and 5 difficult) and 10 negative (5 easy and 5 difficult) scenes. The boxcar functions of each regressor spanned the observation (4 s) and rating period (8 s). Each regressor was convoluted with a canonical hemodynamic response function. Moreover, six movement parameters from the rigid-body transformation of the motion-correction procedure were entered as covariates in the GLM. The voxel-based time series were filtered with a high-pass filter (time constant = 128 s).

### Representational similarity analysis

We employed an RSA to characterize the geometry of neural representations of perceived valence while observing different affective interactions. Representational dissimilarity matrices (RDMs) characterize the pairwise dissimilarity of activation patterns evoked by all observed emotional interactions and, therefore, allow a direct comparison between representational spaces from the behavioral measures and fMRI activation patterns by mapping the correspondence between their similarity structures. For this analysis, we used the toolbox from Nili et al. (2014). For each ROI, all pairwise comparisons were assembled in an RDM. Our first step was to estimate the true activity patterns by applying multivariate noise normalization to the beta coefficients obtained for each stimulus (Walther et al. 2016). In the second step, we calculated the cross-validated Mahalanobis distance to quantify the dissimilarity between each stimulus pair, resulting in a 20 × 20 representational dissimilarity matrix (RDM) (10 positive scenes, 10 negative scenes; see Fig. 1b). Cross-validation was achieved by using the six runs as inputs for a six-fold cross-validation procedure. RDMs were calculated separately for each experimental run and averaged for each subject. This yielded 20 brain RDMs (one per subject) for each of the 10 ROIs that were used to calculate the average similarity between activity patterns across participants. Then, we used multidimensional scaling (MDS) to project the high dimensional RDM space onto two dimensions and gain a graphical impression of representational distances. For this purpose, the 20 subject RDMs were averaged to obtain a single RDM per ROI.

### Association between valence rating and its neural representation

We tested the association between the subjectively perceived valences and the geometry of neural representations that might cause them. For this purpose, we first created rating dissimilarity matrices (rating DMs) representing the structure of the stimulus ratings for each stimulus. For each subject, we compared the mean stimulus valence ratings to each other by calculating the absolute difference between them. This difference served as the dissimilarity, again leading to a 20 × 20 rating DM. To compare brain and behavioral RDMs, we used Pearson's product-moment correlation coefficients and a one-sided signed-rank test across the single-subject RDM correlations. To test differences between fits across ROIs, we used two-sided signed-rank tests across subjects for each pair of brain RDMs. To account for multiple testing, we controlled the false-discovery rate at 0.05. The amount of variance in the behavioral response that a brain RDM can explain is limited by the variability across subjects and indicated by a noise ceiling (gray bar, Fig. 3d).

### Decoding stimulus valence

In a last step, we carried out a multi-voxel pattern analysis (MVPA) in order to analyze whether the neural patterns during observation were distinct enough to decode the observed experimental condition. To assess the specific response patterns within a specific ROI, we employed a support vector machine (SVM). The analysis included leave-one-run-out cross-validation for each subject and ROI. To reduce the number of features, we applied a principal component analysis. In each iteration of the cross-validation, we split the corresponding vectors into a set of tests (one run out of six) and training data (all remaining runs), with 100 vectors (5 runs × 20 stimuli). SVM was provided with labels indicating each condition of the training samples, a decision boundary was extracted based on these data, and this boundary was applied to predict the condition of the test data. We compared each of the assigned valence labels and counted correct and incorrect assignments as 1 and 0. The whole procedure was repeated until each run had served as test data. Then, we calculated the proportion of correct assignments across the six-folds of the cross-validation process. This proportion was derived for each subject and each ROI.

To assess the significance of the decoding accuracies, we conducted a permutation analysis involving random labeling of the valence condition (positive vs. negative interaction). This approach offers a more robust evaluation of statistical significance compared to a one-sample t-test against chance (cf. Stelzer et al. 2013). Across 2000 iterations per subject and ROI, the condition labels for the 100 data samples (training data) underwent random shuffling. The classification accuracy of this randomly labeled dataset was then computed using the leave-one-run-out cross-validation approach outlined earlier. Probability values were determined by calculating the proportion of random shuffles that resulted in an accuracy equal to or greater than the one observed for the actual (unshuffled) labels. All *P*-values underwent correction for multiple ROIs using the Holm–Bonferroni method (Holm 1979).

## Results

### Parametric analysis

Prior to multivariate analyses, we conducted a parametric modulation analysis to determine which brain sites were modulated by the perceived stimulus valence. Results revealed no valence-dependent variation of neural activation with respect to the magnitude. No brain areas were found to show either a positive or negative correlation with the perceived valence (FWE-corrected).

### Multivariate fMRI results

#### *Representational similarity analysis*

Visual inspection of MDS plots (Fig. 2) showed a spatial organization of positive and negative interactions within the IPL, IFG, vPMC, and dPMC (Fig. 2b). In these regions, positive and negative

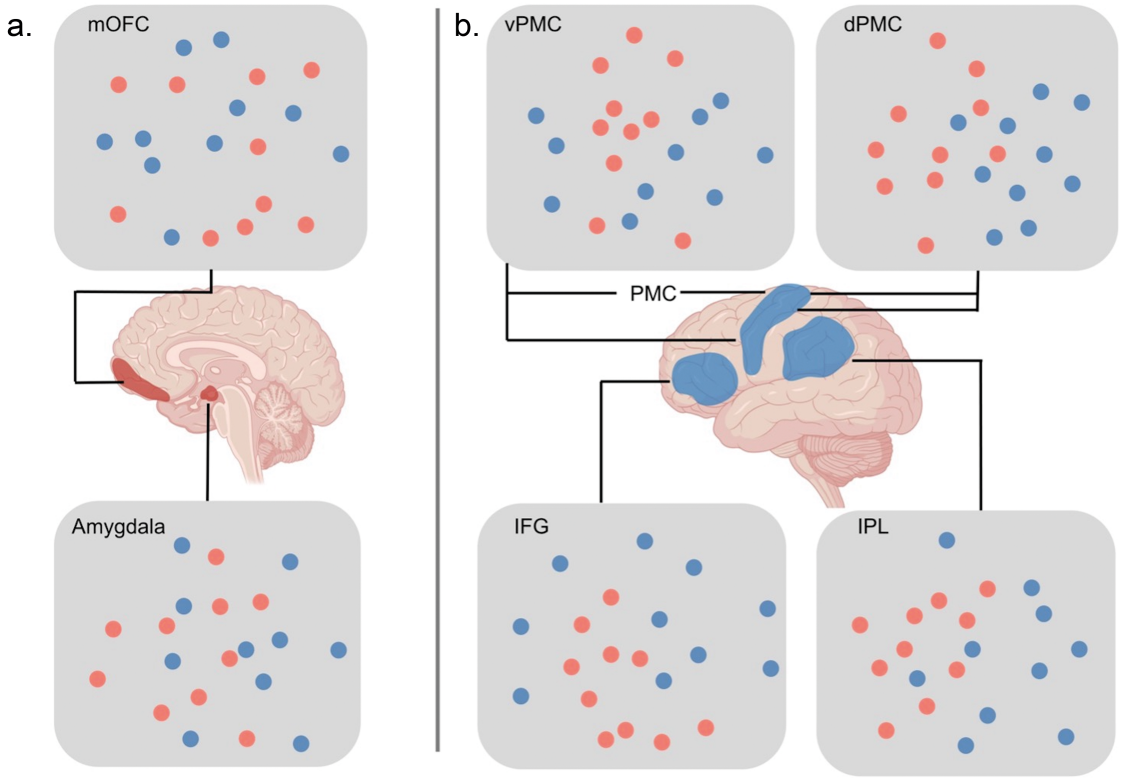


**Figure 2.** MDS plots of brain RDMs. For each ROI, an MDS plot (minimizing metric stress) shows the similarities of the neural pattern elicited by positive (blue) or negative (red) social interactions. The closer the dots are to each other, the more similar their neural patterns. The brain in the middle shows the anatomic location of ROI labels. (a) valence-sensitive regions & (b) Action-Observation Network.

interactions were nearly separated into two clusters in which especially the perceived negative scenes were located closer to each other and thus showed a more similar pattern than perceived positive scenes. This was especially true for the IPL. MDS plots of the mOFC and the amygdala revealed that the scenes were not as sharply separated as in the AON areas (Fig. 2a).

### *Subjective valence representations*

Cross-subject results yielded a behavioral RDM with a high degree of similarity within but not between the two valence categories (Fig. 3b), showing that subjects were able to distinguish very reliably between positive and negative interactions. The described high similarity in the behavioral ratings can be seen in the near upper (Pearson's $r = 0.85$) and lower (Pearson's $r = 0.83$) bounds of the noise ceiling.

Via RSA, we aimed to explore whether the perceived valence (subject ratings) could be explained by the neural geometry of the investigated ROIs. Results showed that the RDM of the left IPL correlated significantly with the rating RDM. It should also be noted that IPL RDM correlated significantly more strongly with perceived valence than all other investigated brain RDMs (Fig. 3d; Table 1). Other AON areas whose RDMs correlated significantly with the behavioral RDM were the RDMs of the IFG, the dPMC, the vPMC, and the STS of both hemispheres, as well as the RDM of the left SPL. It should be noted that the brain RDM of the left and right IFG and the left dPMC also correlated more strongly with the behavioral RDM than all remaining brain RDMs (Fig. 3d). The brain RDM of the amygdala and the mOFC of both hemispheres also correlated significantly with the behavioral RDM, but to a significantly lesser degree than the RDMs of nearly all AON regions. All other investigated brain RDMs did not correlate significantly with the behavioral RDM. All results are reported in Table 1, and remaining RDMs can be found in Supplementary Fig. S2.

### *Decoding*

To investigate whether the neural patterns in the investigated ROIs were distinct enough to differentiate between the observed positive and negative interactions, a decoding was carried out. Regarding the stimulus valence, a significant classification was possible only for the left IPL (Fig. 3c). Accuracies and SEM for decoding results are reported in Table 1.

## Discussion

We found that neural patterns within the AON—specifically, within the IPL and IFG, as well as within the dPMC and vPMC—display a neural geometry reflecting the valence impression of observed PLD interactions. Notably, the IPL demonstrates a distinct valence-dependent gradient, transitioning from the highest similarity between the negative scenes to the lowest similarity between the negative and positive scenes. This neural signature in the IPL is crucial for the successful decoding of the affective content of the observed scenes. Interestingly, areas often associated with valence processing (i.e. the mOFC and the amygdala) do not allow a decoding of stimulus valence, and their representational geometry reflects to a lesser extent the valence impression of the observed scenes compared to AON areas. Our findings also indicate that it is not the activation magnitude within AON and valence-sensitive regions that reflects the perceived valence of PLD interactions but the representational codes.

This study highlights the specific role of the IPL within the AON in deciphering the emotional valence of observed interactions. The representational geometry of the IPL most closely reflects the

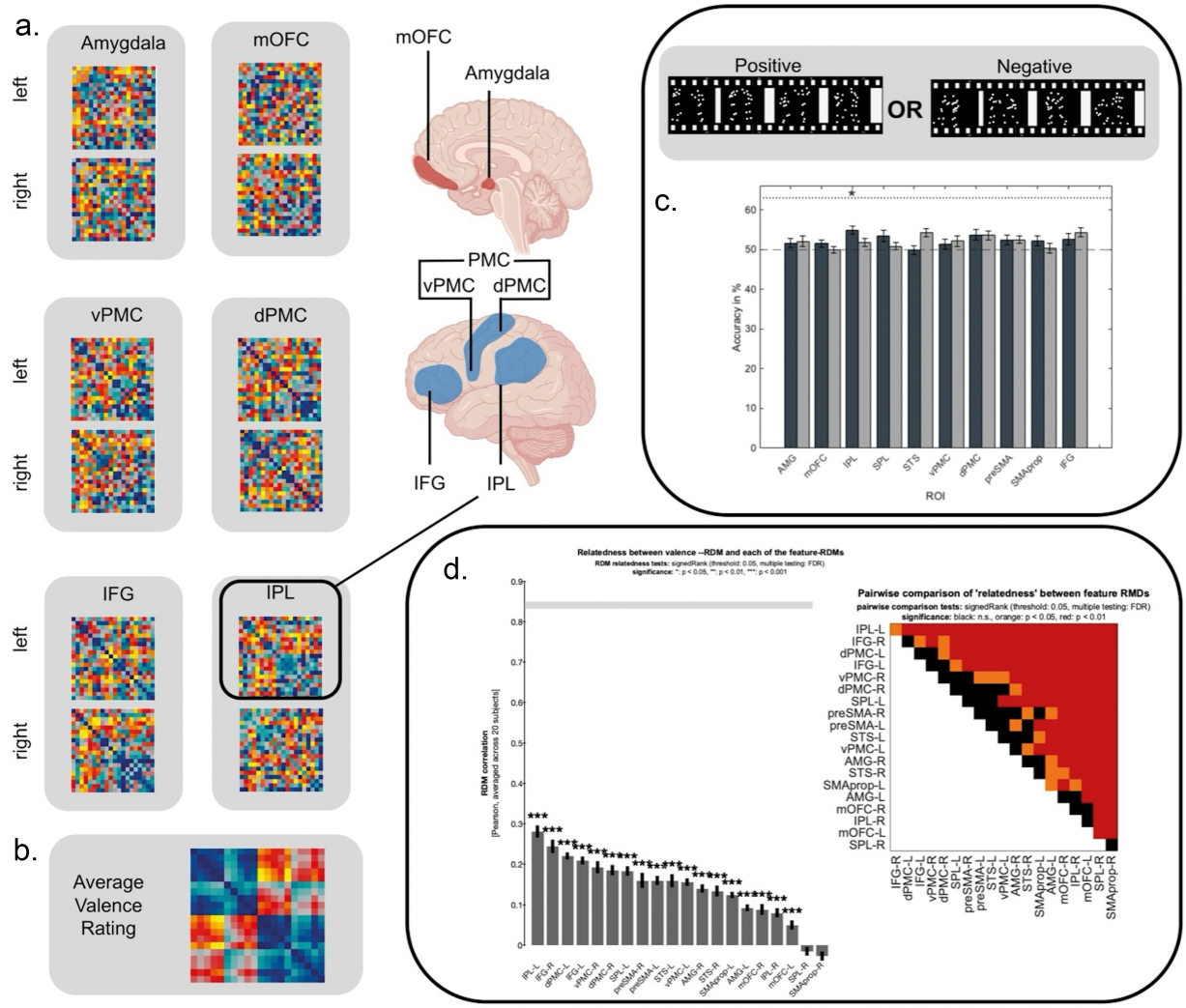


**Figure 3.** Representational dissimilarity matrices, decoding accuracies, and relationship between neural RDMs and valence rating RDMs. (A) Neural RDMs for left and right amygdala, mOFC, vPMC, dPMC, IFG, and IPL (Mahlanaobis distance as similarity measure). (B). Valence rating RDM averaged across participants (absolute distance as similarity measure). (C) Decoding accuracies for each investigated ROI and permutation analysis. Significant correlations shown by asterisks (*$p < .05$). (D). Pearson linear correlations between valence rating RDMs and averaged neural RDMs. Significant correlations shown by asterisks ( *$p < .05$; **$p < .01$; ***$p < .001$, controlling FDR at .05). Lower and upper bounds of the noise ceiling are depicted by a gray bar. Pairwise comparisons indicate which neural RDMs perform significantly differently. Color corresponds to significance level (black = not significant; orange = $p < .05$; red = $p < .01$; calculated via two-sided signed-ranks test across subjects, controlling false-discovery rate at .05).

perceived emotional valence of the scenes, indicating its crucial role in perceiving valence in kinematic stimuli. Areas traditionally associated with processing emotional valence and subjective affect appear to have a secondary role in the present task.

## The AON: valence coding when perceiving kinematics of emotional interactions

It has been suggested that the AON plays an important role in understanding other people's actions and their underlying intentions by integrating observed actions with the personal motor repertoire (Caspers et al. 2010). The IPL plays a key role in this. It is known to be relevant for the sensory-to-motor mapping of visual input (i.e. an observed action) onto the observer's body coordinates (Buccino et al. 2004). Neural activity within the IPL can even use subtle kinematic features of observed acts to discriminate between different intentions (Koul et al. 2018, Patri et al. 2020). Regarding the processing of EBL, several neurophysiological studies have demonstrated that the IPL plays a prominent role in processing emotional content of human actions (Sinke et al. 2010, Engelen et al. 2018). Whereas univariate studies underline the notion that the IPL exhibits a sensitivity toward the processing of negative emotions (Engelen et al. 2015, 2018, Meeren et al. 2016, Poyo Solanas et al. 2018), multivariate studies further indicate that it exhibits emotion-specific stimulus-independent representations (Downing and Peelen 2011, Cao et al. 2018).

This study elucidates that the IPL exhibits distinct neural response patterns associated with negative and positive scenes. The analysis further demonstrates that the neural geometry of the left IPL is best aligned with the behavioral RDM. Specifically, the IPL's neural codes for observed negative scenes show a high degree of similarity, whereas codes for negative and positive scenes show a notable dissimilarity, thus reflecting the rating behavior of participants. These findings underscore that the IPL's neural geometry represents both the affective content of scenes as well as the perceived affect. The pronounced similarity in neural patterns for negative scenes

**Table 1.** Decoding accuracies and RDM correlations. Average decoding accuracy and standard error of the mean regarding the distinction between positive and negative valence of a scene. Pearson linear correlation coefficients between brain regions and perceptual RDMs and their respective standard error of the mean.

| | | Decoding | | RSA | |
|---|---|---|---|---|---|
| ROI | L/R | Accuracy (%) | SEM | Correlation to behavioral RDM | SEM |
| Amygdala | L | 51.62 | 1.17 | 0.10 | 0.01 |
| | R | 52.06 | 1.30 | 0.14 | 0.01 |
| mOFC | L | 52.46 | 1.23 | 0.05 | 0.01 |
| | R | 52.46 | 1.01 | 0.09 | 0.01 |
| IPL | L | **55.01** | 1.00 | **0.28** | 0.02 |
| | R | 51.71 | 1.03 | 0.08 | 0.01 |
| SPL | L | 49.87 | 1.15 | 0.18 | 0.02 |
| | R | 54.17 | 1.03 | −0.02 | 0.02 |
| STS | L | 51.45 | 1.26 | 0.16 | 0.02 |
| | R | 52.15 | 1.31 | 0.13 | 0.01 |
| vPMC | L | 52.63 | 1.37 | 0.16 | 0.01 |
| | R | 54.34 | 1.12 | 0.20 | 0.02 |
| dPMC | L | 53.73 | 1.28 | 0.22 | 0.01 |
| | R | 53.55 | 1.11 | 0.18 | 0.01 |
| preSMA | L | 52.24 | 1.22 | 0.16 | 0.01 |
| | R | 50.35 | 1.30 | 0.16 | 0.02 |
| SMAprop | L | 53.46 | 1.38 | 0.12 | 0.01 |
| | R | 50.83 | 0.89 | −0.03 | 0.02 |
| IFG | L | 51.49 | 0.85 | 0.21 | 0.01 |
| | R | 49.87 | 0.85 | 0.24 | 0.02 |

suggests that the IPL is particularly attuned to negative emotional content within human actions. Affective actions articulate specific expressions of an individual's needs and intentions, thereby also enabling the prediction of future behaviors (Flanagan and Johansson 2003, Wilson and Knoblich 2005). This capability, especially in recognizing negative emotions, is vital for ensuring one's physical and psychological safety (Baumeister et al. 2001, Vaish et al. 2008). This suggests that the IPL may have evolved a specialized adaptation for processing negative affect.

The IPL is suggested to be a shared neural substrate between action and perception and, thus, involved in the process of internal simulation (Rizzolatti et al. 2006). Recent findings underscore its role in processing spatiotemporal contingencies of social interactions and generating somatosensory representations of body states with perceived emotions (Ross and Atkinson 2020, Atkinson and Vuong 2023). Our findings underlie the importance of the IPL in the process of understanding kinematic information with emotional content through simulation.

The RSA revealed additional AON sites exhibiting a representational geometry that, to some extent, maps the valence impressions of the observed scenes. The neural pattern in the IFG as well as vPMCs and dPMCs correlated strongly with the behavioral RDMs. Yet, the patterns in these regions—specifically, in the IFG and both the dorsal and ventral sections of the PMC—were not sufficiently distinct to decode the content of the observed stimulus.

The IFG is, like the IPL, involved in action understanding (Iacoboni et al. 2005, Rizzolatti et al. 2006, Li et al. 2020), thereby inferring intentions and action outcomes (Buccino et al. 2004, Patri et al. 2020). It is particularly active when observing complex and goal-directed actions (Caspers et al. 2010), whole-body actions, and interactions, but less active when observing independently acting individuals (cf. Caspers et al. 2010, Centelles et al. 2011). Furthermore, the IFG has a specific sensitivity to emotions transported via body language (Saygin et al. 2004, Gazzola et al. 2007, Keuken et al. 2011, Quadflieg and Koldewyn 2017).

It becomes apparent that neural responses of both regions—the IFG and the IPL—are modulated by action intention as well as by emotion in actions (Keuken et al. 2011, Ansuini et al. 2015, Cao et al. 2018). A recent study by Patri et al. (2020) tried to clarify the specific roles of the IFG and the IPL in action observation. It found that disruption of activity in the IPL, but not in the IFG, impaired an observer's ability to interpret the intentional significance of changes in discriminative kinematic features. This provides causal support for an architecture in which especially the IPL represents goals or intentions during action observation. This observation could account for our result that the IPL outperformed the IFG and other AON regions in representing the affective intention of the observed kinematic stimuli.

Besides the IPL and IFG, the PMC displays the affective valuation of the observed scenes. The PMC exhibits a particular sensitivity for emotional body movements (Grèzes et al. 2007, Pichon et al. 2009, Sinke et al. 2010), as well as for social scenes, thereby underscoring the notion that it contains a tuning to more complex action representations than meaningless movements (Centelles et al. 2011). Hoshi and Tanji (2006) have further demonstrated that important functions of the PMC are to match motor acts with sensory inputs (vPMC) and to plan and prepare for potential actions the observer might need to perform in response (dPMC). Whereas the IFG and the PMC areas are both central nodes of the AON and active during the observation of (emotional) actions, their roles might differ to a certain degree. The IFG is more involved in the cognitive and interpretative aspects of action observation, focusing on understanding the meaning and intentions behind actions (Iacoboni et al. 2005). In contrast, the PMC is involved more directly in the motor aspects, including the simulation, prediction, and preparation to imitate the observed action or to respond to it appropriately (Fogassi et al. 2005, Molenberghs et al. 2012). Therefore, the better representation of the affective content within the IPL and the IFG compared to the PMC in the present task of observing affective PLD interactions might be explained by the fact that subjects did not have to react to the observed scene. The present task is more about understanding the content of the PLD scenes than preparing an action. This might be especially facilitated by the stimuli used here. The observation of kinematic PLD stimuli, which have a certain degree of abstraction, can further reduce the urge to (re)act.

## Valence-sensitive areas when observing biological motion in social interactions

Limbic areas such as the amygdala and several cortical areas such as the OFC often reveal increased activity when affective valence is being represented during emotion experience and perception, pain, aversion, and orgasm [see Lindquist et al. (2012) for a review]. Studies examining the neural processing of EBL also showed an involvement of the OFC (Pichon et al. 2009, Sinke et al. 2010) and the amygdala (Pichon et al. 2009, Mattek et al. 2020). For example, Pichon et al. (2009) showed an increased BOLD response in the OFC when observing angry compared to fearful stimuli in a person presented from a frontal viewpoint. Similarly, several studies revealed an increased amygdala activation, especially when participants observed full-light displays of fearful or angry bodies (Hadjikhani and De Gelder 2003, Hortensius et al. 2017), thereby underlining the notion that the amygdala is a central node for the neural processing of negative affect (especially fear- and anger-related stimuli) (LeDoux 2003). However, our data

revealed that neural activation within neither the amygdala nor the OFC is modulated when perceiving an interaction that is more negative. Furthermore, it was not possible to decode the positive or negative valence of a scene, and the neural geometry of AON areas more accurately reflects the perceived valence rather than the neural geometry of valence-sensitive areas.

The present experiment's findings suggest that valence perception is less apparent in valence-sensitive areas and more pronounced in AON regions. This distinction may arise from the different types of stimuli used compared to those in other studies. For instance, previous experiments often employed stimuli that either evoked emotional responses directly in observers or used images and videos of people displaying emotions—typically negative ones—from a frontal view (Pichon et al. 2009, Chikazoe et al. 2014). In contrast, our experiment utilized kinematic depictions of human movements observed from a third-person perspective, because we aimed to explore how movement information from others can contribute to perceiving emotional valence. It seems possible that these depictions of interactions from a third-person perspective may not evoke strong feelings of pleasure or discomfort in observers due to their abstract nature and that they therefore might not engage the amygdala in assessing signal relevance (de Gelder 2006). This observation aligns with findings from studies employing PLDs, which also did not report amygdala activation in response to affective actions (Heberlein and Saxe 2005, Centelles et al. 2011, Atkinson et al. 2012).

## Conclusion

The present study investigated whether AON and valence-sensitive regions convey valence information when processing EBL depicted by kinematic stimuli. Our findings show that a decoding of stimulus valence is possible within the IPL, thereby suggesting a distinctiveness of the neural codes underlying the observation of positive and negative scenes. Furthermore, we observed that the neuronal geometry of AON and valence-sensitive areas, albeit to a lesser degree, reflects the geometry of subjective valence ratings as indicated by RSA. We found the closest match of neural activation patterns and behavioral responses within the IPL. Because this cortical site is considered as representing action intention from observed kinematics, the accentuated role of the IPL in the present study can also be explained by the notion that the decoding of affect via kinematic stimuli is a form of intention recognition.

## Acknowledgements

Magnetic Resonance Imaging for this study was performed at the Bender Institute of Neuroimaging at the Justus-Liebig-University Giessen, Germany. The authors thank Jonathan Harrow for his helpful comments.

## Supplementary data

Supplementary data is available at *SCAN* online

Conflict of interest: None declared.

## Funding

This article was funded by the Deutsche Forschungsgemeinschaft, Germany (IRTG 1901—The Brain in Action).

## Data availability

All data are available upon request.

## References

Ansuini C, Cavallo A, Koul A *et al*. Predicting object size from hand kinematics: a temporal perspective. *PLoS One* 2015;**10**:e0120432. https://doi.org/10.1371/journal.pone.0120432

Atkinson AP, Vuong QC. Incidental visual processing of spatiotemporal cues in communicative interactions: an fMRI investigation. *Imaging Neurosci* 2023;**1**:1–25. https://doi.org/10.1162/imag_a_00048

Atkinson AP, Vuong QC, Smithson HE. Modulation of the face- and body-selective visual regions by the motion and emotion of point-light face and body stimuli. *NeuroImage* 2012;**59**:1700–12. https://doi.org/10.1016/j.neuroimage.2011.08.073

Bachmann J, Munzert J, Krüger B. Neural underpinnings of the perception of emotional states derived from biological human motion: a review of neuroimaging research. *Front Psychol* 2018;**9**:1763. https://doi.org/10.3389/fpsyg.2018.01763

Baumeister RF, Bratslavsky E, Finkenauer C *et al*. Bad is stronger than good. *Rev General Psychol* 2001;**5**:323–70. https://doi.org/10.1037/1089-2680.5.4.323

Buccino G, Binkofski F, Riggio L. The mirror neuron system and action recognition. *Brain Lang* 2004;**89**:370–76. https://doi.org/10.1016/S0093-934X(03)00356-0

Cao L, Xu J, Yang X *et al*. Abstract representations of emotions perceived from the face, body, and whole-person expressions in the left postcentral gyrus. *Front Hum Neurosci* 2018;**12**:419. https://doi.org/10.3389/fnhum.2018.00419

Carrington SJ, Bailey AJ. Are there theory of mind regions in the brain? A review of the neuroimaging literature. *Hum Brain Mapp* 2009;**30**:2313–35. https://doi.org/10.1002/hbm.20671

Caspers S, Zilles K, Laird AR *et al*. ALE meta-analysis of action observation and imitation in the human brain. *NeuroImage* 2010;**50**:1148–67. https://doi.org/10.1016/j.neuroimage.2009.12.112

Centelles L, Assaiante C, Nazarian B *et al*. Recruitment of both the mirror and the mentalizing networks when observing social interactions depicted by point-lights: a neuroimaging study. *PLoS One* 2011;**6**:e15749. https://doi.org/10.1371/journal.pone.0015749

Chikazoe J, Lee DH, Kriegeskorte N *et al*. Population coding of affect across stimuli, modalities and individuals. *Nat Neurosci* 2014;**17**:1114–22. https://doi.org/10.1038/nn.3749

Clarke TJ, Bradshaw MF, Field DT *et al*. The perception of emotion from body movement in point-light displays of interpersonal dialogue. *Perception* 2005;**34**:1171–80. https://doi.org/10.1068/p5203

Decatoire A, Beauprez S-A, Pylouster J *et al*. PLAViMoP: how to standardize and simplify the use of point-light displays. *Behav Res Methods* 2019;**51**:2573–96. https://doi.org/10.3758/s13428-018-1112-x

de Gelder B. Towards the neurobiology of emotional body language. *Nat Rev Neurosci* 2006;**7**:242–49. https://doi.org/10.1038/nrn1872

de Gelder B, De Borst AW, Watson R. The perception of emotion in body expressions. *WIREs Cogn Sci* 2015;**6**:149–58. https://doi.org/10.1002/wcs.1335

De Meijer M. The contribution of general features of body movement to the attribution of emotions. *J Nonverbal Behav* 1989;**13**:247–68. https://doi.org/10.1007/BF00990296

Destrieux C, Fischl B, Dale A *et al*. Automatic parcellation of human cortical gyri and sulci using standard anatomical nomenclature. *NeuroImage* 2010;**53**:1–15. https://doi.org/10.1016/j.neuroimage.2010.06.010

Downing PE, Peelen MV. The role of occipitotemporal body-selective regions in person perception. *Cogn Neurosci* 2011;**2**:186–203. https://doi.org/10.1080/17588928.2011.582945

Engelen T, De Graaf TA, Sack AT *et al*. A causal role for inferior parietal lobule in emotion body perception. *Cortex* 2015;**73**:195–202. https://doi.org/10.1016/j.cortex.2015.08.013

Engelen T, Zhan M, Sack AT *et al*. Dynamic interactions between emotion perception and action preparation for reacting to social threat: a combined cTBS-fMRI study. *eNeuro* 2018;**5**:ENEURO.0408-17.2018. https://doi.org/10.1523/ENEURO.0408-17.2018

Flanagan JR, Johansson RS. Action plans used in action observation. *Nature* 2003;**424**:769–71. https://doi.org/10.1038/nature01861

Fogassi L, Ferrari PF, Gesierich B *et al*. Parietal lobe: from action organization to intention understanding. *Science* 2005;**308**:662–67. https://doi.org/10.1126/science.1106138

Frijda NH. *The Emotions*. Cambridge, England: Cambridge University Press; Editions de la Maison des Sciences de l'Homme, 1986.

Gallagher HL, Frith CD. Functional imaging of 'theory of mind'. *Trends Cogn Sci* 2003;**7**:77–83. https://doi.org/10.1016/S1364-6613(02)00025-6

Gazzola V, Rizzolatti G, Wicker B *et al*. The anthropomorphic brain: the mirror neuron system responds to human and robotic actions. *NeuroImage* 2007;**35**:1674–84. https://doi.org/10.1016/j.neuroimage.2007.02.003

Grèzes J, Pichon S, de Gelder B. Perceiving fear in dynamic body expressions. *NeuroImage* 2007;**35**:959–67. https://doi.org/10.1016/j.neuroimage.2006.11.030

Grossman ED, Blake R. Brain activity evoked by inverted and imagined biological motion. *Vis Res* 2001;**41**:1475–82. https://doi.org/10.1016/S0042-6989(00)00317-5

Hadjikhani N, De Gelder B. Seeing fearful body expressions activates the fusiform cortex and amygdala. *Curr Biol* 2003;**13**:2201–05. https://doi.org/10.1016/j.cub.2003.11.049

Heberlein AS, Saxe RR. Dissociation between emotion and personality judgments: convergent evidence from functional neuroimaging. *NeuroImage* 2005;**28**:770–77. https://doi.org/10.1016/j.neuroimage.2005.06.064

Holm S. A simple sequentially rejective multiple test procedure. *Scand J Stat* 1979;**6**:65–70.

Hortensius R, Terburg D, Morgan B *et al*. The dynamic consequences of amygdala damage on threat processing in Urbach-Wiethe Disease. A commentary on Pishnamazi et al. (2016). *Cortex* 2017;**88**:192–97. https://doi.org/10.1016/j.cortex.2016.07.013

Hoshi E, Tanji J. Differential involvement of neurons in the dorsal and ventral premotor cortex during processing of visual signals for action planning. *J Neurophysiol* 2006;**95**:3596–616. https://doi.org/10.1152/jn.01126.2005

Hutton C, Bork A, Josephs O *et al*. Image distortion correction in fMRI: a quantitative evaluation. *NeuroImage* 2002;**16**:217–40. https://doi.org/10.1006/nimg.2001.1054

Iacoboni M, Molnar-Szakacs I, Gallese V *et al*. Grasping the intentions of others with one's own mirror neuron system. *PLoS Biol* 2005;**3**:e79. https://doi.org/10.1371/journal.pbio.0030079

Johansson G. Visual perception of biological motion and a model for its analysis. *Percept Psychophys* 1973;**14**:201–11. https://doi.org/10.3758/BF03212378

Keck J, Zabicki A, Bachmann J *et al*. Decoding spatiotemporal features of emotional body language in social interactions. *Sci Rep* 2022;**12**:15088. https://doi.org/10.1038/s41598-022-19267-5

Keuken MC, Hardie A, Dorn BT *et al*. The role of the left inferior frontal gyrus in social perception: an rTMS study. *Brain Res* 2011;**1383**:196–205. https://doi.org/10.1016/j.brainres.2011.01.073

Koul A, Cavallo A, Cauda F *et al*. Action observation areas represent intentions from subtle kinematic features. *Cereb Cortex* 2018;**28**:2647–54. https://doi.org/10.1093/cercor/bhy098

Kret ME, Pichon S, Grèzes J *et al*.. Similarities and differences in perceiving threat from dynamic faces and bodies. An fMRI study. *NeuroImage* 2011a;**54**:1755–62. https://doi.org/10.1016/j.neuroimage.2010.08.012

Kret ME, Pichon S, Grèzes J *et al*. Men fear other men most: gender specific brain activations in perceiving threat from dynamic faces and bodies—an fMRI study. *Front Psychol* 2011b;**2**:3. https://doi.org/10.3389/fpsyg.2011.00003

Kuppens P, Tuerlinckx F, Russell JA *et al*. The relation between valence and arousal in subjective experience. *Psychol Bull* 2013;**139**:917–40. https://doi.org/10.1037/a0030811

LeDoux J. The emotional brain, fear, and the amygdala. *Cell Mol Neurobiol* 2003;**23**:727–38. https://doi.org/10.1023/a:1025048802629

Li X, Krol MA, Jahani S *et al*. Brain correlates of motor complexity during observed and executed actions. *Sci Rep* 2020;**10**:10965. https://doi.org/10.1038/s41598-020-67327-5

Lindquist KA, Satpute AB, Wager TD *et al*. The brain basis of positive and negative affect: evidence from a meta-analysis of the human neuroimaging literature. *Cereb Cortex* 2016;**26**:1910–22. https://doi.org/10.1093/cercor/bhv001

Lindquist KA, Wager TD, Kober H *et al*. The brain basis of emotion: a meta-analytic review. *Behav Brain Sci* 2012;**35**:121–43. https://doi.org/10.1017/S0140525X11000446

Lorey B, Kaletsch M, Pilgramm S *et al*. Confidence in emotion perception in point-light displays varies with the ability to perceive own emotions. *PLoS One* 2012;**7**:e42169. https://doi.org/10.1371/journal.pone.0042169

Mattek AM, Burr DA, Shin J *et al*. Identifying the representational structure of affect using fMRI. *Affect Sci* 2020;**1**:42–56. https://doi.org/10.1007/s42761-020-00007-9

Meeren HKM, Hadjikhani N, Ahlfors SP *et al*. Early preferential responses to fear stimuli in human right dorsal visual stream—a MEG study. *Sci Rep* 2016;**6**:24831. https://doi.org/10.1038/srep24831

Molenberghs P, Cunnington R, Mattingley JB. Brain regions with mirror properties: a meta-analysis of 125 human fMRI studies. *Neurosci Biobehav Rev* 2012;**36**:341–49. https://doi.org/10.1016/j.neubiorev.2011.07.004

Nili H, Wingfield C, Walther A *et al*. A toolbox for representational similarity analysis. *PLoS Comput Biol* 2014;**10**:e1003553. https://doi.org/10.1371/journal.pcbi.1003553

Ongür D, Price JL. The organization of networks within the orbital and medial prefrontal cortex of rats, monkeys and humans. *Cereb Cortex* 2000;**10**:206–19. https://doi.org/10.1093/cercor/10.3.206

Patri J-F, Cavallo A, Pullar K *et al*. Transient disruption of the inferior parietal lobule impairs the ability to attribute intention to action. *Curr Biol* 2020;**30**:4594–605.e7. https://doi.org/10.1016/j.cub.2020.08.104

Pichon S, De Gelder B, Grèzes J. Two different faces of threat. Comparing the neural systems for recognizing fear and anger in dynamic

body expressions. *NeuroImage* 2009;**47**:1873–83. https://doi.org/10.1016/j.neuroimage.2009.03.084

Pollick FE, Paterson HM, Bruderlin A *et al*. Perceiving affect from arm movement. *Cognition* 2001;**82**:B51–61. https://doi.org/10.1016/S0010-0277(01)00147-0

Poyo Solanas M, Zhan M, Vaessen M *et al*. Looking at the face and seeing the whole body neural basis of combined face and body expressions. *Soc Cogn Affect Neurosci* 2018;**13**:135–44. https://doi.org/10.1093/scan/nsx130

Quadflieg S, Koldewyn K. The neuroscience of people watching: how the human brain makes sense of other people's encounters. *Ann NY Acad Sci* 2017;**1396**:166–82. https://doi.org/10.1111/nyas.13331

Rizzolatti G, Ferrari PF, Rozzi S *et al*. The inferior parietal lobule: where action becomes perception. In: Chadwick DJ, Diamond M and Goode J (eds.), *Novartis Foundation Symposia*. Vol. **270**, 1st edn. Hoboken, New Jersey, U.S.: Wiley, 2006, 129–45. https://doi.org/10.1002/9780470034989.ch11

Ross P, Atkinson A. Expanding simulation models of emotional understanding: the case for different modalities, body-state simulation prominence and developmental trajectories. *Front Psychol* 2020;**11**:309. https://doi.org/10.3389/fpsyg.2020.00309

Saxe R. Uniquely human social cognition. *Curr Opin Neurobiol* 2006;**16**:235–39. https://doi.org/10.1016/j.conb.2006.03.001

Saygin AP, Wilson SM, Hagler DJ *et al*. Point-light biological motion perception activates human premotor cortex. *J Neurosci* 2004;**24**:6181–88. https://doi.org/10.1523/JNEUROSCI.0504-04.2004

Schwarzlose RF, Baker CI, Kanwisher N. Separate face and body selectivity on the fusiform gyrus. *J Neurosci* 2005;**25**:11055–59. https://doi.org/10.1523/JNEUROSCI.2621-05.2005

Sinke CBA, Sorger B, Goebel R *et al*. Tease or threat? Judging social interactions from bodily expressions. *NeuroImage* 2010;**49**:1717–27. https://doi.org/10.1016/j.neuroimage.2009.09.065

Small DM, Gregory MD, Mak YE *et al*. Dissociation of neural representation of intensity and affective valuation in human gustation. *Neuron* 2003;**39**:701–11. https://doi.org/10.1016/S0896-6273(03)00467-7

Stelzer J, Chen Y, Turner R. Statistical inference and multiple testing correction in classification-based multi-voxel pattern analysis (MVPA): random permutations and cluster size control. *NeuroImage* 2013;**65**:69–82. https://doi.org/10.1016/j.neuroimage.2012.09.063

Vaish A, Grossmann T, Woodward A. Not all emotions are created equal: the negativity bias in social-emotional development. *Psychol Bull* 2008;**134**:383–403. https://doi.org/10.1037/0033-2909.134.3.383

Wallbott HG. Bodily expression of emotion. *Eur J Social Psychol* 1998;**28**:879–96. https://doi.org/10.1002/(SICI)1099-0992(1998110)28:6<879::AID-EJSP901>3.0.CO;2-W

Walther A, Nili H, Ejaz N *et al*. Reliability of dissimilarity measures for multi-voxel pattern analysis. *NeuroImage* 2016;**137**:188–200. https://doi.org/10.1016/j.neuroimage.2015.12.012

Wilson M, Knoblich G. The case for motor involvement in perceiving conspecifics. *Psychol Bull* 2005;**131**:460–73. https://doi.org/10.1037/0033-2909.131.3.460

Social Cognitive and Affective Neuroscience, 2025, 20(1), nsaf021, DOI: https://doi.org/10.1093/scan/nsaf021, Advance Access Publication Date: 15 February 2025, Original Research – Neuroscience
Received: 29 May 2024; Revised: 17 September 2024; Accepted: 13 February 2025